Journal of Medicinal Chemistry

pubs.acs.org/jmc

Article

Enhancing Bioactivity of *N,N,N*-Chelating Rhodium(III) Complexes with Ionic Liquids: Toward Targeted Cancer Therapy

Angelina Caković, Dušan Ćoćić, Marko Živanović, Nenad Janković, Nevena Milivojević, Marija Delibašić, Marina Kostić, Ivana Radojević, Mirjana Grujović, Katarina G. Marković, Olivera R. Klisurić, Milan Vraneš, and Jovana Bogojeski*

Cite This: *J. Med. Chem.* 2024, 67, 13349−13362

Read Online

ACCESS | Metrics & More | Article Recommendations | Supporting Information

ABSTRACT: This study investigates the potential of using ionic liquids as cosolvents to enhance the solubility and activity of poorly soluble rhodium(III) complexes, particularly those with diene, pyridine derivatives, and camphor-derived bis-pyrazolylpyridine ligands, in relation to 5′-GMP, CT-DNA, and HSA as well as their biological activity. Findings indicate that ionic liquids significantly increase the substitution activity of these complexes toward 5′-GMP while only marginally affecting DNA/HSA binding affinities with molecular docking, further confirming the experimental results. Lipophilicity assessments indicated good lipophilicity. Notably, cytotoxicity studies show that **Rh2** is selectively effective against HeLa cancer cells, with IL1 and IL10 modulating the cytotoxic effects. Redox evaluations indicate that rhodium complexes induce oxidative stress in cancerous cells while maintaining redox balance in noncancerous cells. By elucidating the role of ionic liquids in modulating these effects, the study proposes a promising avenue for augmenting the efficacy and selectivity of cancer treatments, thus opening new horizons in cancer therapeutics.

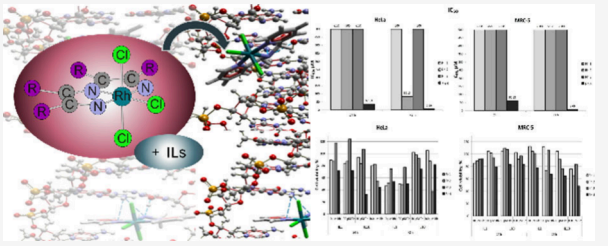

INTRODUCTION

Transitional metal complexes have played a crucial role in the treatment and diagnosis of cancer, owing to the success of cisplatin in cancer therapy worldwide.[1−3] However, not many transition complexes besides cisplatin are used in cancer therapy because of their toxic effects, poor solubility, and the development of resistance.[4] The toxic effects of cisplatin and the resistance to its application are the main reasons for the worldwide investigation of different metal complexes as anticancer agents.[4] Metals like rhodium, ruthenium, osmium, and iridium are especially interesting in this area of research.[5−10] At the early stages of anticancer research, rhodium was not considered interesting to the public due to its inert nature. However, since the 70s, there has been a growing interest in the potential of rhodium complexes as anticancer agents. This interest has evolved from binuclear rhodium(II) complexes to mononuclear species that contain Rh(I) and finally Rh(III) ions.[11−17] Rhodium complexes are unequivocally one of the most promising potential anticancer agents available today.[17−19] Their inertness provides the opportunity for a complex design that can specifically target molecules, such as DNA, proteins, or enzymes, making them highly versatile and effective in fighting cancer.

The interaction between transition metal complexes and DNA molecules is an essential and exciting research area in bioinorganic chemistry, medicine, and pharmacy. Its potential to unlock new treatment methods for various diseases, including cancer treatment, is undeniable.[20,21] The DNA molecule is one of the primary intracellular targets for the activity of anticancer transition metal complexes, with the possibility of interacting by intercalation, groove binding, or electrostatic interactions.[17,22−25] The potential use of transition metal complexes in therapy is significantly limited by a key drawback: the tendency of these metals to form sparingly soluble complexes. This drawback severely restricts their efficacy and is a major challenge that must be overcome to realize their full potential in medical treatment. One way to enhance complexes' solubility is through using cosolvents. Among these, ionic liquids (ILs) have emerged as a particularly viable option, earning them the nickname "green solvents of the future".[26,27] Composed entirely of ions and possessing low melting points, ILs are less harmful than conventional organic solvents and are considered ecologically sound. Thanks to their ion-based composition, these solvents can be modified to be nontoxic and biocompatible with the human body. The most famous ILs consist of cations like choline and different biocompatible anions.[27−29] Given their unique properties,

Received: May 28, 2024
Revised: July 12, 2024
Accepted: July 19, 2024
Published: July 26, 2024

ionic liquids have the potential to be highly effective cosolvents for sparingly soluble complexes that exhibit anticancer activity. The fact that ILs are ecofriendly and less harmful than conventional organic solvents and that they can be modified to be nontoxic and biocompatible with the human body makes them a promising option for enhancing the solubility of such complexes.

In this research, we explore the influence of nontoxic cosolvents (ILs) on the structure−activity relationship of rhodium(III) complexes containing *N*,*N*,*N*-ligands toward DNA and HSA molecules, as well as 5′-GMP molecules, and assess their impact on biological activity.

RESULTS AND DISCUSSION

Synthesis and Characterization. The structures of the examined Rh(III) complexes are illustrated in Figure 1. The

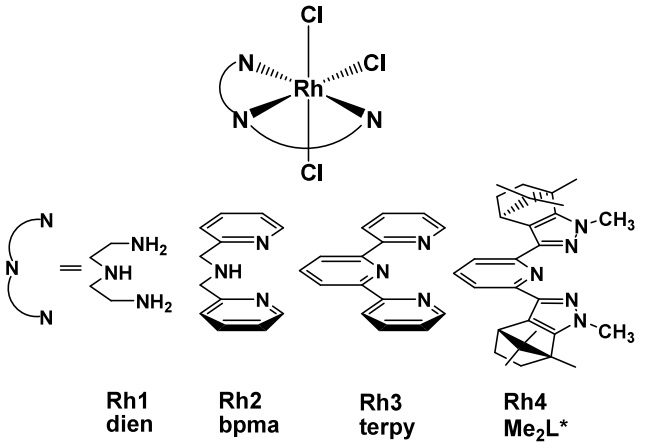

Figure 1. Structural formulas of the investigated **Rh1−4** complexes.

complex **Rh2** was synthesized and characterized in this work, whereas the complexes **Rh1**, **Rh3**, and **Rh4** were synthesized according to previously published procedures.[14,30,31] The **Rh2** complex was synthesized by stirring equimolar amounts of $RhCl_3 \cdot xH_2O$ and bpma (bis(pyridin-2-ylmethyl)amine) ligand in ethanol, followed by refluxing overnight. The synthesized complex was characterized by NMR spectroscopy, elemental analysis, and X-ray diffraction. The elemental analysis results closely matched the proposed composition of the complex. The NMR spectra of the complex indicated the formation of a single, distinct species. Additionally, single crystals of the **Rh2** complex, suitable for X-ray diffraction analysis, were obtained. Further details are provided in the Experimental Section.

It is worth noting that the selection process began with the diene type, followed by complexes that feature pyridine and then camphor.[14] Pyridine is known for its π-back-donation,[32,33] which heightens the electrophilicity of the metal center and can improve its binding affinity. The fourth complex that is examined contains camphor-derived bis-pyrazolylpyridine. Camphor, known for its historical use in certain cultures for perceived medicinal benefits, has found its way into topical products due to its cooling sensation and is occasionally utilized for its decongestant properties.

Table 1 contains information on the structures and names of the examined ionic liquids (ILs). It is important to mention that IL1 was obtained commercially, and IL2−11 are nontoxic ionic liquids that were synthesized according to published procedures.[34,35] Notably, IL2−7 belong to the choline-based

Table 1. Structures and Names of the Investigated Ionic Liquids

Name	Cation	Anion	
1-ethyil-3-methylimid-azolium ethyl sulfate	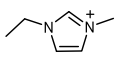	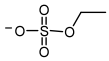	IL1
choline nicotinate	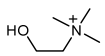	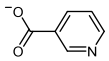	IL2
choline biotinate	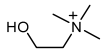	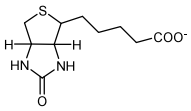	IL3
choline gamma-aminobutyr-ate	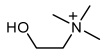	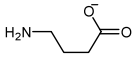	IL4
choline ascorbate	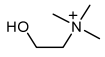	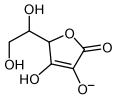	IL5
choline syringate	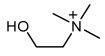	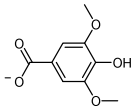	IL6
choline benzoate	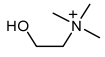	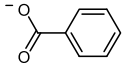	IL7
agmatine nicotinate	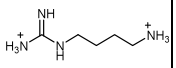	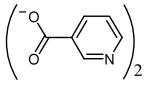	IL8
agmatine ascorbate	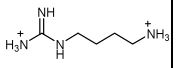	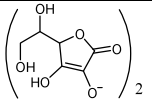	IL9
agmatine salicylate	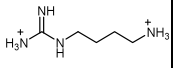	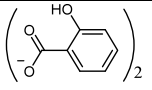	IL10
agmatine ibuprofenate	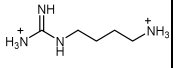	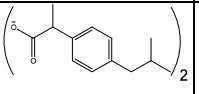	IL11

family of ionic liquids, whereas IL8−11 are classified as agmatine-based ionic liquids.[36]

Crystal Structure Analysis. The crystallographic structure of complex $[Rh(bpma)Cl_3]$ (**Rh2**) with the adopted atom-numbering scheme is shown in Figure 2. Complex **Rh2** crystallizes in the triclinic crystal system and $P\bar{1}$ space group, in which the asymmetric part of the unit cell contains one neutral molecule. Selected bond lengths, bond angles, and dihedral angles of **Rh2** are listed in Table S1.

The geometrical structure of complex **Rh2** is best defined by the coordination of **Rh2** and the angle between the mean

https://doi.org/10.1021/acs.jmedchem.4c01220
J. Med. Chem. 2024, 67, 13349−13362

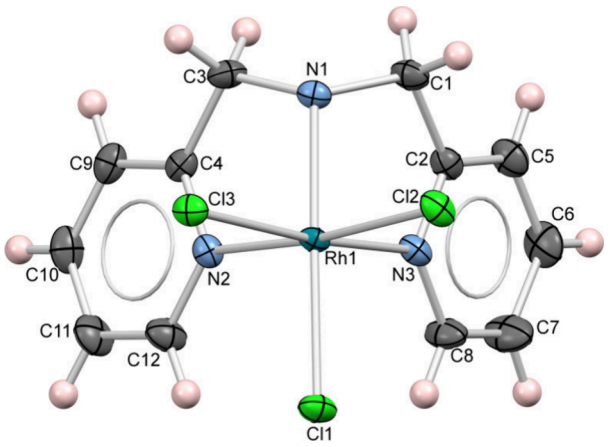

Figure 2. MERCURY[37] drawing of the molecular structure of complex **Rh2** with labeled non-H atoms. Displacement ellipsoids are shown at 30% probability.

planes of the phenyl rings (Table S1). The rhodium(III) center in the [Rh(bpma)Cl_3] complex is coordinated in a slightly distorted octahedral geometry. The tridentate *N,N,N*-donor from the bpma (bis(pyridin-2-ylmethyl)amine) ligand coordinates facially to the rhodium(III) core, and the other three positions are occupied by chlorine atoms. The *N,N,N*-donor from the bpma ligand is involved in chelation to form two five-membered rings.

Comparing the bond lengths (Table S1) of the coordinated nitrogen atoms, one can notice slight variations in the lengths of Rh−N bonds [from 2.023 (3) to 2.053 (3) Å] where the axial nitrogen is placed at the longest distance from the metal center. The same can be concluded when it comes to chlorine atoms, where the Rh−Cl bond lengths vary from 2.3519 (10) to 2.3544 (11) Å (Table S1).

The two phenyl rings of the bpma ligand are nearly perpendicular, as confirmed by the value 83.37 (2)° of the angle between their mean planes. Other conformation parameters are given in Tables S1 and S2.

Kinetic Studies. The reactivity of complexes **Rh1−4** (Figure 1) was measured by performing substitution reactions with 5′-GMP under physiological conditions with different ILs as cosolvents. By examining the substitution with 5′-GMP, it is possible to assess the potential for coordination with DNA molecules. Consequently, DNA emerges as a prospective target for the activity of the investigated complexes.[14,23,35]

The substitution reaction of the labile chloride ligand was followed by using UV−vis spectroscopy, where the changes in absorbance were measured as a function of time at pH = 7.2 (25 mM HEPES buffer/50 mM NaCl) and T = 310 K. The proposed reaction pathways for all observed substitution processes of the examined complexes **Rh1−4** are presented in Scheme 1. The nucleophile concentrations were kept at least 10-fold in excess to ensure accurate results, allowing the reactions to be studied under pseudo-first-order conditions.

The experiments aimed to evaluate the effect of ionic liquids, specifically IL1−11, on the constant values of k_2 of the substitution reactions. To achieve this, the reactions were conducted with ionic liquids as cosolvents, added in the same amount as the studied complexes to maintain the same concentrations (ratio 1:1, conc. 1×10^{-4} M). Displayed in Table 2 are the substitution rate constants, which were determined using pseudo-first-order conditions. These values

Scheme 1. Schematic Representation of the Substitution Reactions for the Complexes Rh1−4 with 5′-GMP as a Nucleophile

$$[RhLCl_3] + Nu \underset{k_1}{\overset{k_2}{\rightleftharpoons}} [RhLNuCl_2]^+ + Cl^-$$

L= dien, bpma, terpy, MeL

Nu= 5′-GMP

Table 2. Rate Constants of the Substitution Reactions of the Complexes Rh1−4 with 5′-GMP in the Presence of Ionic Liquids IL1−11 and DMF as Cosolvents (Complex−Ionic Liquid Ratio Was 1:1, 1×10^{-4} M) at pH = 7.2 (25 mM HEPES Buffer) in the Presence of 50 mM NaCl

	Rh1	Rh2	Rh3	Rh4
	$10^5 k_2$ (M^{-1} s^{-1})	$10^5 k_2$ (M^{-1} s^{-1})	$10^5 k_2$ (M^{-1} s^{-1})	$10^5 k_2$ (M^{-1} s^{-1})
DMF	0.32 ± 0.01	0.19 ± 0.02	0.40 ± 0.01	0.78 ± 0.01
IL1	3.95 ± 0.02	2.90 ± 0.02	3.10 ± 0.03	5.24 ± 0.01
IL2	3.93 ± 0.01	4.46 ± 0.01	4.93 ± 0.01	6.93 ± 0.04
IL3	4.11 ± 0.03	3.29 ± 0.01	3.60 ± 0.01	4.84 ± 0.03
IL4	4.13 ± 0.01	1.52 ± 0.01	1.70 ± 0.01	3.16 ± 0.03
IL5	3.33 ± 0.03	1.66 ± 0.02	2.10 ± 0.01	3.45 ± 0.01
IL6	4.06 ± 0.01	3.44 ± 0.04	3.80 ± 0.01	5.34 ± 0.02
IL7	2.91 ± 0.01	1.84 ± 0.02	2.40 ± 0.01	3.42 ± 0.02
IL8	0.71 ± 0.02	0.72 ± 0.04	1.30 ± 0.01	2.35 ± 0.01
IL9	1.31 ± 0.01	1.03 ± 0.03	1.50 ± 0.03	2.85 ± 0.01
IL10	0.80 ± 0.02	0.47 ± 0.01	0.70 ± 0.02	1.53 ± 0.02
IL11	0.93 ± 0.03	0.63 ± 0.01	0.90 ± 0.02	2.17 ± 0.01

were obtained by plotting the linear relationship between k_{obsd} and the total nucleophile concentration (eq S1). By examination of the slope of the k_{obsd} vs nucleophile concentration graph, the second-order rate constant (k_2) can be calculated, providing insight into product formation.

Cosolvents play a crucial role in the solubility and stability of sparingly soluble complexes. In this study, ionic liquids were found to be effective cosolvents for **Rh1−4** complexes. The substitution rate constant values for all studied complexes increased significantly when ionic liquids were used, surpassing even the standard organic solvent DMF. Notably, the addition of only a small amount of ionic liquids to the solution was enough to enhance the solubility of the tested complexes, and higher concentrations can be achieved if needed, owing to the nontoxic properties of the ionic liquids.

Among the ionic liquids tested, IL2−7 containing choline ions were found to be the most effective in increasing the constant values, specifically IL4 and IL3 for **Rh1** and IL2 and IL6 for **Rh2−4**. The electronic and steric impacts of the ionic liquids were found to play a crucial role in substitution, facilitating the departure of chloride ions, stabilizing the complex, and improving coordination with the 5′-GMP molecule. Interestingly, the tested ILs did not stop but instead enhanced the coordination of the 5′-GMP molecule to **Rh1−4** complexes, making them ideal cosolvents for sparingly soluble complexes. Furthermore, the tested ionic liquids are nontoxic, making them ideal for biological applications. IL2−11 contain biologically friendly cations (choline and agmatine) and anions (nicotinate, ascorbate, biotinate, etc.), which are nontoxic to the human body, while IL1 was commercially obtained for

https://doi.org/10.1021/acs.jmedchem.4c01220
J. Med. Chem. 2024, 67, 13349−13362

comparison. The results show that the constant values k_2 of complexes **Rh1−4** for IL2−7 were higher than those for IL1, while those for IL8−11 were lower. In conclusion, the tested ionic liquids are effective cosolvents for sparingly soluble complexes and can be used to enhance their solubility and even their biological activity. The biocompatible and nontoxic properties of these ionic liquids make them ideal for biological applications, and their effectiveness in increasing constant values makes them a promising alternative to conventional organic solvents.

DNA Binding Studies. *Electronic Absorption Method.* Electronic absorption spectroscopy is frequently employed when investigating the bonding between complexes and DNA. The nature of the interaction between transition metal complexes and DNA can be covalent or noncovalent.[38,39] By examining the changes in the absorption spectra of the complex in response to increasing DNA concentration, it is possible to determine the type of interaction occurring. These changes may include a hypochromic shift, a hyperchromic shift in absorption intensity, and a slight shift in the absorption wavelength maximum.[20,40] To further explore the effect of using ionic liquids as cosolvents in the interaction between complexes **Rh1−4** and DNA, absorption titration studies were conducted. The measurements at room temperature were taken with a fixed complex/ionic liquid concentration (ratio of 1:2, 8 μM) and varying amounts of DNA up to a ratio of 5.[35,41] It is important to note that ionic liquids do not interact with DNA independently, which was considered to ensure the reliability of the results.

The complexes **Rh1−4** were investigated and found to have a constant order of 10^4, indicating moderate interaction with DNA. Previous research provided the K_b values for complexes **Rh3** and **Rh4** in the presence of DMF as a cosolvent. The results presented in Table 3 show that ionic liquids had a minor effect on the K_b values, with the constant order remaining unchanged from when DMF was used. Additionally, the values in the presence of ionic liquids containing agmatine ion, IL8−11, were significantly lower than those observed in the presence of ionic liquids containing choline ion, IL2−7. For complexes **Rh1** and **Rh2**, all ILs resulted in a slight increase in the binding constant values. However, for complexes **Rh3** and **Rh4**, a slight decrease in value was observed from previously published results.[13,14] The highest value of the binding constant for complex **Rh1** was observed in the presence of IL3 and IL4, while for complexes **Rh2−4**, the highest value was observed in the presence of IL2 and IL6, which is consistent with the kinetic results. These findings suggest that ionic liquids had a limited effect on the DNA interaction of complexes **Rh1−4**, with K_b values remaining in the same order of reactivity of 10^4.

Table 3. DNA Binding Constants, K_b, for the Examined Complexes Rh1−4 in the Presence of DMF and Ionic Liquids IL1−11 as Cosolvents (Complex−Ionic Liquid Ratio Was 1:2) in PBS

	Rh1	Rh2	Rh3	Rh4
	10^4K_b (M^{-1})	10^4K_b (M^{-1})	10^4K_b (M^{-1})	10^4K_b (M^{-1})
DMF	2.6 ± 0.1	4.1 ± 0.1	7.0 ± 0.1	8.3 ± 0.1
IL1	2.9 ± 0.1	4.7 ± 0.1	4.3 ± 0.1	5.2 ± 0.1
IL2	2.8 ± 0.1	4.9 ± 0.1	4.6 ± 0.1	5.6 ± 0.1
IL3	3.1 ± 0.1	4.6 ± 0.1	4.5 ± 0.1	5.4 ± 0.1
IL4	3.4 ± 0.1	4.3 ± 0.1	4.1 ± 0.1	5.2 ± 0.1
IL5	2.8 ± 0.1	4.5 ± 0.1	4.2 ± 0.1	5.3 ± 0.1
IL6	2.6 ± 0.1	4.7 ± 0.1	4.5 ± 0.1	5.5 ± 0.1
IL7	2.7 ± 0.1	4.4 ± 0.1	4.4 ± 0.1	5.1 ± 0.1
IL8	2.2 ± 0.1	4.3 ± 0.1	3.8 ± 0.1	4.7 ± 0.1
IL9	2.5 ± 0.1	4.1 ± 0.1	3.9 ± 0.1	4.9 ± 0.1
IL10	2.4 ± 0.1	4.2 ± 0.1	3.7 ± 0.1	4.6 ± 0.1
IL11	2.5 ± 0.1	4.2 ± 0.1	4.1 ± 0.1	4.5 ± 0.1

The bulky structure of the DNA molecule is likely the primary factor that has limited the increase in the constant value. However, increasing the concentration of ionic liquids can potentially overcome this limitation and lead to a substantial increase in the value. Although the DNA structure and the small concentration of the applied ILs present some challenges, they are still highly promising candidates for the cosolvents of the examined complexes.

Fluorescence Spectroscopic Methods. It is worth noting that while absorption spectroscopic measurements can confirm the interaction between a complex and a DNA molecule,[42] fluorescence measurements are a far more reliable method for determining the binding mode. Intercalation, a type of DNA interaction, can be determined using fluorescence quenching titrations with ethidium bromide (EB), a classical intercalator. EB exhibits low fluorescence intensity in solution, but upon intercalation between the DNA chains, it displays a significant intensity of fluorescence emission at around 612 nm.[40,43]

Confirming the interaction between the tested complex and DNA through intercalative mode relies heavily on the complex's ability to intercalate more effectively than EB. By displacing the EB molecule in a DNA−EB cluster, the complex causes a decrease in the fluorescence emission of the solution, which serves as a trustworthy indicator of intercalation.[42,44−46] Hence, a reduction in fluorescence intensity is a reliable indicator of whether the examined complex interacts with DNA via an intercalative mode.

The investigation aimed to determine the impact of using ionic liquids as cosolvents on the ability of complexes **Rh1−4** to interact with DNA. To achieve this objective, fluorescence quenching titrations with EB were conducted in the presence of ionic liquids IL1−11, with a constant concentration of DNA−EB cluster solution (ratio of DNA to EB is 1:1, 5 μM) while increasing the concentration of **Rh1−4** complexes (up to a ratio of 5). Throughout the process, the emission intensity of the DNA−EB cluster solution was monitored, and the Stern−Volmer constants for complexes **Rh1−4** in the presence of cosolvents are listed in Table 4.

The results in Table 4 demonstrate that all applied ILs exhibit a minor impact on the K_{sv} constant. The constants remained in the same order of reactivity, which was 10^4, indicating that the presence of ILs barely affected the interactions via the intercalative mode. The UV−vis and fluorescence spectroscopic measurements showed a good stacking of acquired values, thereby confirming the reliability of the data. For the complexes **Rh3** and **Rh4**, good value stacking was observed in line with already published results, further validating the findings. A slight increase in binding constant values when using IL1−7 and a slight decrease in the value when using IL8−11 can be observed for all examined complexes. The highest constant value for IL4 (**Rh1**) and IL2 (**Rh2−4**) is in accordance with the kinetic and UV−vis spectroscopic measurements, providing a more robust understanding of the study's findings.

https://doi.org/10.1021/acs.jmedchem.4c01220
J. Med. Chem. 2024, 67, 13349−13362

Table 4. Stern−Volmer Constants, K_{sv}, for the Examined Complexes Rh1−4 in the Presence of DMF and Ionic Liquids IL1−11 as Cosolvents (Complex−Ionic Liquid Ratio Was 1:2, 16 μM) in PBS

	Rh1	Rh2	Rh3	Rh4
	10^4K_{sv} (M^{-1})	10^4K_{sv} (M^{-1})	10^4K_{sv} (M^{-1})	10^4K_{sv} (M^{-1})
DMF	2.2 ± 0.1	3.4 ± 0.1	3.8 ± 0.1	5.5 ± 0.1
IL1	2.6 ± 0.1	3.7 ± 0.1	4.2 ± 0.1	5.6 ± 0.1
IL2	2.5 ± 0.1	3.8 ± 0.1	4.4 ± 0.1	5.9 ± 0.1
IL3	2.6 ± 0.1	3.6 ± 0.1	4.3 ± 0.1	5.8 ± 0.1
IL4	2.7 ± 0.1	3.4 ± 0.1	3.9 ± 0.1	5.6 ± 0.1
IL5	2.4 ± 0.1	3.5 ± 0.1	4.1 ± 0.1	5.7 ± 0.1
IL6	2.3 ± 0.1	3.6 ± 0.1	4.3 ± 0.1	5.8 ± 0.1
IL7	2.3 ± 0.1	3.5 ± 0.1	4.2 ± 0.1	5.5 ± 0.1
IL8	2.0 ± 0.1	3.4 ± 0.1	3.6 ± 0.1	5.2 ± 0.1
IL9	2.2 ± 0.1	3.2 ± 0.1	3.7 ± 0.1	5.3 ± 0.1
IL10	2.1 ± 0.1	3.3 ± 0.1	3.5 ± 0.1	5.2 ± 0.1
IL11	2.3 ± 0.1	3.3 ± 0.1	3.8 ± 0.1	5.1 ± 0.1

Viscosity Measurements. Viscosity measurements are crucial in identifying DNA binding patterns. In classical intercalation, the insertion of a compound between DNA bases unequivocally results in an increase in the length of the DNA chain, thereby leading to a corresponding rise in the solution's viscosity.[23,47,48] The degree of intercalation is directly proportional to the increase in DNA viscosity. Experiments were conducted to confirm that the tested complexes bind via intercalation as their DNA interaction method and to test the effect of using ILs on DNA interactions. To measure the viscosity of DNA solutions, complexes **Rh1−4** were added in increasing concentrations in the presence of IL4 as a cosolvent for **Rh1** and IL2 for **Rh2−4** (Figure 3). It was determined that

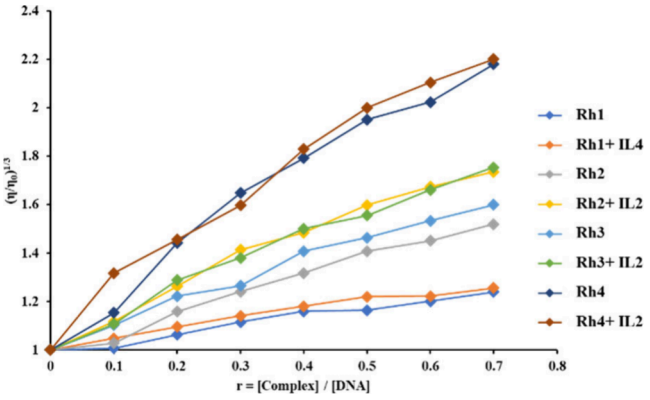

Figure 3. Relative viscosity of the DNA solution in 10 mM PBS in the presence of the complexes **Rh1−4** in the absence and presence of IL of different concentrations (r).

these particular ILs (IL2 and IL4) were the most optimal choice for the study based on the fact that they consistently produced the highest constant values in fluorescence experiments.

The results showed that the relative viscosity of DNA moderately increased with the addition of complex concentrations up to r = 1.0 in a DNA solution (0.01 mM) for **Rh2−4** and slightly increased for **Rh1**. These findings were consistent with the data obtained through UV−vis and fluorescence measurements and the structures of the tested complexes. Complex **Rh1** does not have any rings in its structure compared to **Rh2−4**, which have multiple. It is well-known that, for a compound to intercalate between DNA strands, it must have a voluminous and rigid structure. Usually, complexes intercalate between DNA strands with their organic ligand part, so the results obtained were expected due to the structure of **Rh1**. As the number of rings in the tested complex's structure increased, the viscosity increased in the order of **Rh2** < **Rh3** < **Rh4**, and the difference between **Rh2** and **Rh3** was only slight. Although the presence of ILs slightly increased the solution's viscosity, the data presented in Figure 3 demonstrated that the ILs' presence did not significantly increase the possibility of intercalation of the tested complexes.

In summary, the results obtained through UV−vis, fluorescence spectroscopy, and viscosity measurements confirm that the tested ILs are appropriate cosolvents for the examined complexes. The constant values of all applied biocompatible ion liquids were similar to those obtained in the presence of organic solvents. The presence of the selected ILs did not affect the way of binding of complexes to DNA. The best results for the complex **Rh1** were obtained in the presence of IL4, while the best results for the complexes **Rh2−4** were obtained in the presence of IL2. Although it should be mentioned that all ILs showed similar values, the mentioned ones showed a slightly higher value.

Rhodium complexes were analyzed in two distinct DNA structures: canonical B-DNA (PDB ID: 1BNA) and DNA with an intercalation gap (PDB ID: 1Z3F). This examination allowed for the evaluation of two types of interactions: minor groove and intercalation. The crystal structure of a synthetic DNA dodecamer was represented by fragment 1BNA, while 1Z3F showcased the crystal structure of six base pairs of DNA fragments in a complex with an intercalating anticancer drug ellipticine (which was removed before docking). The highest-ranking poses are presented in Table S3, while the best-docked poses of complexes with DNA are depicted in Figures 4 and S1−S3, based on the scoring functions employed.

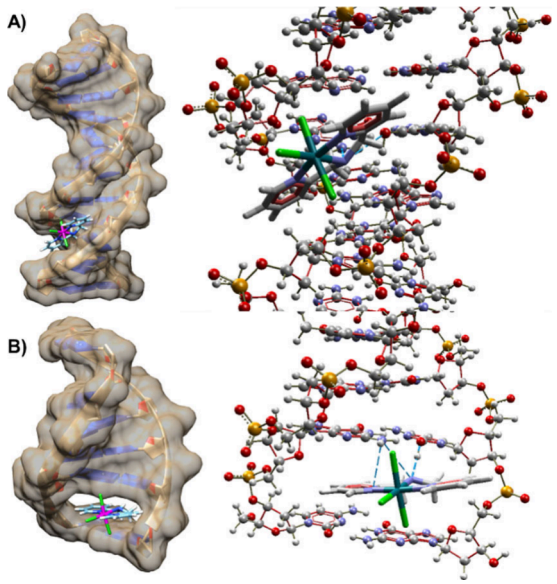

Figure 4. Computational docking model illustrating interactions between complex **Rh2** and DNA (A) with the canonical gap (1BNA) and (B) with the intercalation gap (1Z3F) (dotted lines display a possibility of forming hydrogen bonds).

https://doi.org/10.1021/acs.jmedchem.4c01220
J. Med. Chem. 2024, 67, 13349−13362

According to the scoring functions based on Molegro Virtual Docker (such as MolDock values) outlined in Table S3, the examined complexes appear to have a high degree of structural complementarity with the DNA molecule. Across all complexes analyzed, minor groove binding was found to be generally more effective than intercalation. The scores obtained from Table S3 for intercalation and minor groove binding were ranked as follows: **Rh4** > **Rh3** > **Rh2** > **Rh1**. Complexes containing planar ligands, such as **Rh3** and **Rh4**, have a stronger affinity for DNA structures. Even the presence of a relatively bulky camphor moiety in complex **Rh4** highlights the interactions. Complex **Rh1**, which has the lowest affinity for the DNA helix according to the MolDock scoring function, is best suited for the formation of potential hydrogen bonds that can further stabilize the complex−DNA system.

Fluorescence Spectroscopy of HSA. As the principal protein in the bloodstream, albumin is vital in facilitating the transportation of a wide range of substances throughout the human body. These substances include hormones, fatty acids, ions, drugs, and other essential components, which albumin carries through the blood plasma to various organs and tissues.[49,50] Understanding the interactions between transitional metal complexes and human serum albumin (HSA) proteins is therefore crucial in studying potential drugs, given the critical role albumin plays in this process.[45,51−54]

In this research, the interaction between complexes **Rh1−4** and HSA was explored using fluorescence spectroscopy. To do so, the HSA solution was excited at 295 nm, the wavelength at which fluorescence is solely caused by tryptophan. The examined complexes were then added to the HSA solution in increasing concentrations, resulting in a reduction in fluorescence, indicating an interaction. The reduction in fluorescence observed is likely the result of alterations in the tertiary structure of the protein, induced by modifications in the environment surrounding tryptophan within serum albumin upon binding of the complex.[55] The Stern−Volmer constant (K_{sv}) values were calculated using the Stern−Volmer equation derived from the linear relationship between I_0/I and $[Q]$.[56]

For further reference, Table 5 presents the K_{sv} values for the complexes' interaction with serum albumin, both independently and in the presence of ionic liquids (ILs). Notably, it is observed that all ILs exerted a comparable influence on the constant values throughout the DNA interactions. Consequently, IL2 and IL4 were selected to investigate the HSA interactions of complexes **Rh1−4**, as they yielded the highest constants during the examination of DNA interactions in their presence.

The K_{sv} values in Table 5 indicate that the complexes analyzed interact favorably with HSA. The order of affinity toward HSA, i.e., **Rh4** > **Rh3** ≥ **Rh2** > **Rh1**, is like that of the DNA interactions. Notably, rhodium complexes with larger ligands display higher binding constants for HSA interactions. Additionally, the presence of ILs as cosolvents led to a slight increase in constant values with the most significant enhancement observed in complex **Rh2**. Complexes **Rh2** and **Rh3** exhibited nearly identical constant values in DMF as a cosolvent, but complex **Rh2** had a higher constant value in the presence of IL2 than complex **Rh3**.

Competitive Experiments with HSA and Site Markers. Human serum albumin (HSA) possesses a distinctive heart-shaped structure comprising three domains (I−III), each of which encompasses two subdomains (A and B).[57,58] Specifically, the subdomains IIA and IIIA of HSA are recognized to harbor binding sites for metallo complexes.[59] Competitive experiments using site markers have been conducted to identify the binding site of the analyzed complexes and determine whether they bind to sites I and/or II of the HSA molecules using fluorescence titration. Eosin Y was utilized as a marker for site I of the subdomain IIA, while ibuprofen was a marker for site II of the subdomain IIIA.[59,60]

The fluorescence titration was carried out with an excitation wavelength of 295 nm and an emission range of 300−500 nm. HSA and the markers were added in equimolar concentrations (2×10^{-6} M), and the complexes were gradually added in increasing concentration. The reduction in the fluorescence intensity of the HSA solution following the introduction of the site marker suggests that the marker molecule has successfully attached to the HSA. If the complex and corresponding marker bind to the same site in the site marker−HSA system, the complex must compete with the marker for binding to the HSA. This competition would result in a significant change in the constant value. According to the data analysis in Table 5 using the Scatchard equation, there was a change in the constant value for both site markers. The site marker eosin Y showed a slightly higher effect, indicating that both the complex and corresponding marker bind to the same site in the site marker−HSA system and compete for binding to the HSA. This resulted in a significant change in the constant value. However, the change in the constant value in the presence of ibuprofen could not be excluded; therefore, docking measurements were performed. The measurements confirmed that the complex has binding preferences for both binding sites of the HSA molecule with a slight preference for site I (site IIA). Based on this information, it is believed that the examined complexes primarily bind to site I (site IIA) of the HSA molecule due to hydrophobic interaction, although the role of other interactions, such as hydrogen bonds, electrostatic interactions, van der Waals interactions, and steric contacts, cannot be entirely ruled out.

A molecular docking simulation was also conducted to investigate the interaction between rhodium complexes and HSA. The docking was carried out in subdomains IIA and IIIA of the HSA molecule. Subdomain IIA was found to have a large hydrophobic cavity that can accommodate the drug molecule, which plays a significant role in biomolecule metabolism and transportation. The top-scored values for the examined complexes with HSA protein docked into binding sites IIA

Table 5. Interaction Constants for the Examined Complexes Rh1−4 with HSA and Site Markers in the Presence of DMF and Ionic Liquids IL2 and IL4 as Cosolvents (Complex−Ionic Liquid Ratio Was 1:2, 16 μM) in PBS

		HSA	HSA−eosin Y	HSA−ibuprofen
		10^4K_{sv} (M^{-1})	10^4K_{sv} (M^{-1})	10^4K_{sv} (M^{-1})
Rh1	DMF	1.2 ± 0.1	0.5 ± 0.1	0.8 ± 0.1
	IL4	1.5 ± 0.1	/	/
Rh2	DMF	2.3 ± 0.1	1.1 ± 0.1	1.7 ± 0.1
	IL2	3.5 ± 0.1	/	/
Rh3	DMF	2.4 ± 0.1	1.6 ± 0.1	1.9 ± 0.1
	IL2	2.6 ± 0.1	/	/
Rh4	DMF	3.9 ± 0.1	1.7 ± 0.1	2.1 ± 0.1
	IL2	4.2 ± 0.1	/	/

https://doi.org/10.1021/acs.jmedchem.4c01220
J. Med. Chem. 2024, 67, 13349−13362

and IIIA are presented in Table S4, based on the scoring functions used. Figures 5 and S4−S6 illustrate the best poses according to the H bond scoring function with HSA docked into subdomains IIA and IIIA for the investigated complexes.

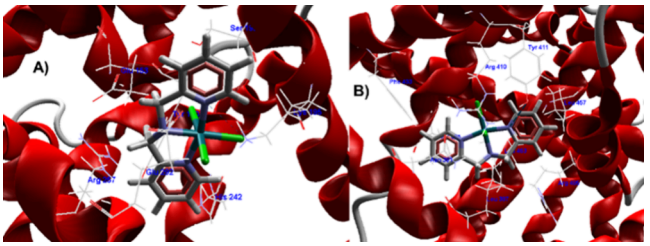

Figure 5. Best pose with HSA docked into a binding pocket for complex **Rh2** according to the H bond values: (A) complexes into the subdomain IIA of HSA protein and (B) complexes into the subdomain IIIA of HSA protein. Selected amino acid residues (selected by applying an energy threshold of 0.625) are represented by stick models (hydrogen bonds are shown as blue dotted lines).

Through investigation, it has been found that rhodium complexes can be accommodated within subdomains IIA and IIIA of an HSA molecule. According to the gain simulation results, subdomain IIA is the more favorable location for hosting the examined complex. This is due, in part, to the larger cavity of subdomain IIA compared to that of the IIIA subdomain, allowing for more voluminous octahedra complexes to be accommodated more effectively. Molecular docking simulations have shown that the affinity order of the complexes toward HSA is **Rh4** > **Rh3** ≥ **Rh2** > **Rh1** for both subdomains. While there is a minor possibility of a hydrogen bond forming between the complexes and amino acid residues of the HSA protein, it was observed to be infrequent.

Lipophilicity Assay. Extensive research has demonstrated that the lipophilicity of metal complexes is a crucial factor in determining their potential biological activity. It is well-established that compounds with a higher lipophilicity tend to have greater cellular uptake, making them more effective as therapeutic agents. Furthermore, the partition coefficient (log P) between the hydrophobic octanol and hydrophilic water phases is a crucial indicator of a compound's lipophilicity and ability to traverse the cell membrane.[61] Notably, log P values for clinically used therapeutic agents, including metal complexes, generally fall within the range from −0.4 to 5.6. Notably, all **Rh1−4** complexes demonstrate log P values that fall within the optimal lipophilicity range of $0 \leq \log P \leq 0.90$. Of particular interest is that **Rh2** and **Rh4** complexes exhibit significantly higher log P values (0.64 and 0.87) than the other two, indicating their preference for the octanol phase. This distinctive characteristic of **Rh2** and **Rh4** complexes also implies their potential as highly efficient therapeutic agents given their superior cellular uptake efficiency.

In Vitro Cytotoxicity Study. In our comprehensive study assessing the cytotoxic potential of novel rhodium complexes, we meticulously quantified their impact on the cell viability in HeLa and MRC-5 cell lines. The half-maximal inhibitory concentration (IC_{50}) serves as a benchmark for cytotoxicity, indicating the potency of a substance in inhibiting a biological process by 50%. Across the four rhodium complexes tested (**Rh1**, **Rh2**, **Rh3**, and **Rh4**), we observed a range of IC_{50} values, revealing a diverse cytotoxic profile (Figure 6).

Rhodium complex **Rh2** demonstrated a particularly potent effect on HeLa cells with an IC_{50} of 85.13 μM after 72 h from treatment, while its influence on MRC-5 was notably less pronounced. This disparity underscores the complex's ability to selectively target cancerous cells while sparing normal, healthy cells. Such a differential could be indicative of the complex's mechanism of action, which may disrupt specific pathways that are more active in cancer cells, hinting at a possibly safer therapeutic window. Complexes **Rh1** and **Rh3** were found to be nontoxic, as indicated by their IC_{50} values, which were greater than 500 μM for both HeLa and MRC-5 cell lines. This suggests that these compounds do not exhibit significant cytotoxicity under the tested conditions. On the other hand, **Rh4** displayed a different profile; despite having very low IC_{50} values for both HeLa and MRC-5 cells, it demonstrated a strong cytotoxic effect. However, it lacked selectivity between the two cell types, indicating that although **Rh4** is toxic, it does not differentiate between cancerous and normal cell lines. To further illustrate the cytotoxic effects, we conducted a time-course study, which revealed that the action of **Rh2** was both time-dependent and dose-dependent, with higher concentrations leading to a more rapid decline in cell viability (Figure S7).

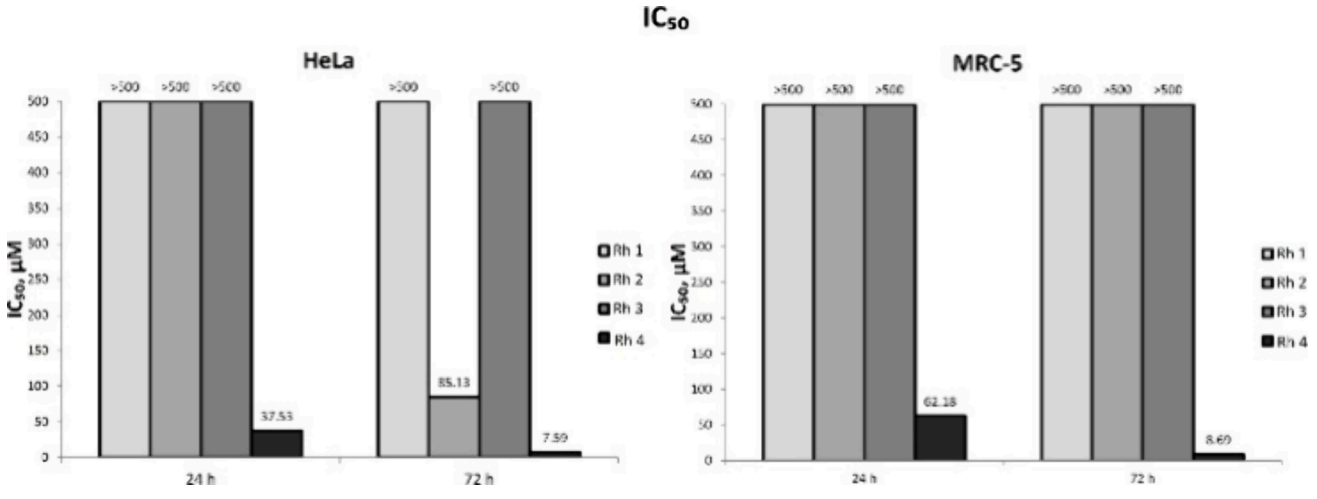

Figure 6. Comparative IC_{50} values of rhodium complexes **Rh1−4** on HeLa and MRC-5 cell lines at 24 and 72 h post-treatment.

https://doi.org/10.1021/acs.jmedchem.4c01220
J. Med. Chem. 2024, 67, 13349−13362

This granular analysis of the cytotoxic effects of rhodium complexes provides a clear indication of their potential as selective anticancer agents. The numerical distinctions between their IC_{50} values offer insight into their therapeutic potential and lay the groundwork for further investigations into their use as targeted treatments for cancer. The specificity of **Rh2** in particular points toward a promising avenue for the development of drugs that could deliver maximum therapeutic effects with minimal impact on healthy tissues. More details on the rhodium complexes' viability influence on HeLa and MRC-5 cells are presented in Figures S7 and S8.

The assessment of ionic liquids (ILs) in our study was predicated on identifying any intrinsic cytotoxic properties that they might exhibit when used independently from rhodium complexes. Employing a fixed concentration of 100 μM for each ionic liquid, we aimed to discern any immediate cytotoxic effects that could be critical for the selection process in further cotreatment assays (Figure S9). Upon analysis, it was observed that IL1 and IL10, out of the series tested, stood out—not for their cytotoxicity but rather for their relatively lower impact on cell viability, marking them as compounds of interest for subsequent experiments. This benchmark of 100 μM was chosen as a hallmark for potential toxicity, and the minimal effects observed suggest that these ILs are suitable candidates for further study in combination treatments without the confounding factor of high inherent cytotoxicity.

The selection of IL1 and IL10 for cotreatment was not solely based on their cytotoxic profile; their chemical significance was also considered. According to the chemical properties and results that are presented in the current data set, it is implied that these ILs possess chemical features that could potentially interact synergistically with the rhodium complexes, altering their bioavailability, stability, or cellular uptake, which in turn could influence the overall therapeutic efficacy of the cotreatment.

The rationale behind the selection process was two-fold: to ensure that the ionic liquids themselves do not exert significant toxicity at the chosen concentration, which could confound the results of cotreatment studies, and to identify ILs that might possess chemical properties conducive to enhancing the anticancer potential of rhodium complexes. The benign cytotoxic profiles of IL1 and IL10 at 100 μM make them ideal candidates for these cotreatment assays, and their chemical significance paves the way for a more nuanced understanding of how ILs can be used to modulate the activity of metal-based therapeutics in cancer treatment.

The comparative cytotoxicity study of rhodium complexes **Rh1**−**4** with and without the cotreatment of ionic liquids IL1 and IL10 reveals a nuanced modulation of their effects on cell viability (Figure S10). The rhodium complexes alone showed a baseline cytotoxic effect on HeLa cells that was altered upon the addition of ionic liquids. On HeLa cells, IL1 generally showed a tendency to decrease cell viability compared to **Rh1** alone, especially after 72 h. Cotreatment with **Rh2** showed a tendency to maintain the cell viability, while cotreatment with **Rh3** and **Rh4** lead to an increase in cell viability. IL10 often resulted in a maintained cell viability except for cotreatment with **Rh2**, where decreased cell viability was observed, indicating an enhancement of the cytotoxic effects. In noncancerous MRC-5 cells, the presence of IL1 and IL10 sometimes led to higher cell viability percentages compared to the treatment with rhodium complexes alone, hinting at a protective effect. The interaction between the ionic liquids and rhodium complexes differed across the specific complex and cell line, with some combinations suggesting the potential for selective targeting of cancer cells. This modulation by IL1 and IL10 suggests that the choice of ionic liquid in cotreatment strategies could be critical in optimizing the therapeutic efficacy and selectivity of rhodium-based cancer treatments.

In Vitro Redox Status Modulation. The modulation of the redox status by rhodium complexes provides pivotal insights into their mechanistic underpinnings as potential anticancer agents. In our study, three key redox parameters, namely superoxide anion radicals, nitrite levels, and glutathione (GSH) content, were meticulously measured to ascertain the oxidative impact of these complexes on HeLa and MRC-5 cell lines.

Upon treatment with rhodium complexes, HeLa cells exhibited a marked increase in superoxide anion radicals, a primary indicator of oxidative stress (Figure S11). These radicals, often precursors to more reactive and damaging species, suggest the initiation of an oxidative cascade that may lead to cellular damage and apoptosis. Similarly, nitrite levels, which can serve as a surrogate marker for the presence of nitric oxide, were elevated, as shown in Figure S12. This increase in nitrites further implicates the rhodium complexes in the promotion of a nitrosative stress environment, which can lead to various forms of nitrosative damage within cellular components. In stark contrast, GSH levels in HeLa cells showed a significant decrease post-treatment, as shown in Figure S13. GSH is a critical antioxidant molecule that quenches free radicals and detoxifies reactive oxygen species (ROS). The depletion of GSH indicates a compromised cellular defense mechanism against the onslaught of oxidative stress, leaving the cells more susceptible to damage and dysfunction.

The changes in redox parameters in MRC-5 cells, however, were less pronounced, pointing toward a differential sensitivity to the rhodium complexes. While there was a slight increase in superoxide anion radicals and nitrite levels (Figures S14 and S15), suggesting the initiation of an oxidative response, the GSH levels did not decrease as substantially as in HeLa cells (Figure S16). This nuanced response underscores the selective toxicity of rhodium complexes, capable of inducing significant oxidative stress in cancerous cells while sparing noncancerous cells, thus maintaining a better redox homeostasis.

The correlation between increased ROS production and cell death in HeLa cells supports the hypothesis that the cytotoxicity of rhodium complexes is mediated through an oxidative stress mechanism. The differential increase in superoxide anion radicals and nitrites, coupled with the depletion of GSH in HeLa cells, suggests that the cancer cells are less equipped to counteract the increased oxidative burden, leading to cell death. In contrast, the MRC-5 cells' ability to maintain higher levels of GSH in the face of rhodium complex-induced oxidative stress may explain their relative resistance to the cytotoxic effects.

This dichotomy in redox status between the cancerous and noncancerous cells is critical for understanding the therapeutic potential of rhodium complexes. It highlights the possibility of exploiting the heightened vulnerability of cancer cells to oxidative damage while minimizing the impact on normal cells. Such selectivity is desirable in anticancer therapy, aiming to maximize the cytotoxic effect on malignant cells while reducing the collateral damage to healthy tissue.

https://doi.org/10.1021/acs.jmedchem.4c01220
J. Med. Chem. 2024, 67, 13349−13362

Further investigations into the precise mechanisms by which rhodium complexes disrupt the redox balance and induce cell death could facilitate the design of targeted cancer treatments. Understanding the interplay among ROS generation, antioxidant depletion, and cellular defenses will be key to optimizing the use of rhodium complexes in clinical settings. This redox-based approach to cancer therapy could form the cornerstone of new, more effective treatments that leverage the inherent biochemical disparities between cancerous and noncancerous cells.

Microbiology. In addition to in vitro testing, the antimicrobial activity of **Rh1−4** complexes was investigated. The studied complexes exhibited moderate to negligible antimicrobial activity, with further details provided in the Supporting Information (Tables S5 and S6 and Figures S17−S20). The antimicrobial activity of the **Rh1−4** complexes was not tested in the presence of ionic liquids. These complexes demonstrated greater antitumor potential compared to their antimicrobial activity, suggesting that future research could focus on their application in cancer treatment.

CONCLUSION

In conclusion, research within this paper has delved into the untapped potential of biocompatible ionic liquids as cosolvents, effectively amplifying the solubility of sparingly soluble rhodium(III) complexes. Our primary aim was to scrutinize the interactions between octahedral rhodium(III) complexes—comprising diene and pyridine derivative ligands, as well as the camphor-derived bis-pyrazolylpyridine ligand—and essential biomolecules such as 5′-GMP, DNA, and HSA in the presence of diverse ionic liquids (IL1−11) and DMF as cosolvents. The substitution reactions involving the examined complexes **Rh1−4** with 5′-GMP revealed that ionic liquids substantially increased the solubility of the complexes, thereby resulting in a notable augmentation of the constant substitution values. Complexes **Rh1−4** showed moderate interaction ability toward CT-DNA and HSA in the presence of IL1−11 and DMF, indicating a minimal influence of the ionic liquids on the complexes−DNA or complexes−HSA binding. Furthermore, assessments of the lipophilicity of the complexes showed good lipophilicity. Docking studies revealed strong structural complementarity between the complexes and DNA, favoring minor groove binding. Also, the complexes exhibited notable affinity for HSA, localized mainly within HSA's subdomain IIA. A docking examination of DNA Gyr and TyrRS interactions highlighted steric effects' significance, with complex **Rh4** showing higher affinity for both DNA Gyr and TyrRS. The intensity of the antimicrobial effect of **Rh1−4** complexes varied depending on the type of microorganisms and the type and concentration of complexes. In general, the rhodium(III) complexes showed highly selective and moderate activity.

Research also elucidated the complex interplay between rhodium complexes and ionic liquids, shedding light on their potential to selectively target cancer cells. The cytotoxicity studies revealed that among the rhodium complexes, **Rh2** stands out with its unique ability to selectively diminish the viability of cancerous HeLa cells while exerting minimal effects on noncancerous MRC-5 cells. This selectivity is a crucial finding, as it suggests the possibility of targeted cancer treatment with reduced side effects on healthy tissue. The addition of ionic liquids IL1 and IL10 further nuances this effect, with IL1 typically decreasing the viability of HeLa cells and IL10 sometimes enhancing the cytotoxic effect of the rhodium complexes. This ability to modulate cytotoxicity through cotreatment opens new avenues for optimizing cancer therapies that are as effective as they are discerning.

The investigation into the redox status of treated cells provided additional insights, with rhodium complexes inducing oxidative stress in cancerous cells, as evidenced by increased superoxide anion radicals and nitrite levels coupled with decreased GSH levels. In contrast, the noncancerous cells maintained a better redox balance, supporting the idea of selective cytotoxicity. The distinct redox responses of cancerous vs noncancerous cells to rhodium complexes highlight the potential for exploiting the unique vulnerabilities of cancer cells. Such targeted therapies could revolutionize cancer treatment, minimizing harm to healthy cells while effectively combating cancerous growths. Our findings lay the groundwork for future studies aimed at unlocking the full therapeutic potential of metal-based complexes in oncology.

EXPERIMENTAL SECTION

Chemicals and Solutions. Phosphate buffer (PBS) (0.01 M, C_{NaCl} = 0.137 M, C_{KCl} = 0.0027 M, pH = 7.4), $RhCl_3{\cdot}xH_2O$, bis(pyridin-2-ylmethyl)amine (bpma), DMF, 1-ethyl-3-methylimidazolium ethyl sulfate (IL1), calf thymus DNA (CT-DNA), eosin Y, ethidium bromide (EB), ibuprofen, and human serum albumin (HSA) were purchased from Sigma-Aldrich and were prepared by dissolving the measured amount of the substance without prior purification. The DNA solution was prepared in 0.01 M phosphate buffer at pH = 7.4, with the ratio of UV absorbance at 260 and 280 nm (A_{260}/A_{280}) between 1.8 and 1.9, indicating that the DNA was liberated from the protein. The concentration of the DNA solution was determined by UV absorption at 260 nm (ε = 6600 M^{-1} cm^{-1}). All solutions were stored at 277 K and used within 5 days. Bidestilated water was used for preparing the solutions. Complexes **Rh1**, **Rh3**, and **Rh4** were synthesized according to the published procedures.[14,30,31] IL2−11 were synthesized according to the published procedures.[34−36]

Instrumental Methods. NMR spectra were recorded on a 200 MHz Varian Gemini-2000 instrument. NMR signals were referenced to residual proton or carbon signals of the deuterated solvent (^{1}H NMR) and are reported in parts per million relative to TMS. Elemental analyses (C, H, and N) were recorded on an Elementar Vario MICRO elemental analyzer. UV−vis and kinetic measurements were conducted on a PerkinElmer Lamda 25 double-beam spectrophotometer with thermostated 1.00 cm quartz Suprasil cells, with the temperature controlled to ±0.1 °C. Fluorescence was measured on an RF-1501 PC spectrofluorometer (Shimadzu, Japan), with the excitation and emission bandwidths both 10 nm. HPLC traces were done on am HPLC-LC20AT instrument, Shimadzu.

Synthesis and Characterization of Complex [Rh(bpma)Cl$_3$], Rh2. Complex [Rh(bpma)Cl_3] (**Rh2**) (Figure 1) was synthesized by stirring one equivalent of $RhCl_3{\cdot}xH_2O$, with one equivalent of bpma (bis(pyridin-2-ylmethyl)amine) in ethanol and refluxing for four hours. Obtained yellow orange participants were filtered and dried under a vacuum. The newly synthesized **Rh2** complex was characterized, and a single crystal of a DMSO adduct suitable for the X-ray analysis was also obtained.

^{1}H NMR (500 MHz, DMSO-d_6): δ = 4.34 (s; 4H; CH_2), 7.47 (m; 2H; py), 7.65 (m; 2H; py), 7.89 (m; 2H; py), 9.22 (d; 2H; py).

Anal. Calcd for $C_{12}H_{13}Cl_3N_3Rh$: C, 35.28; H, 3.21; N: 10.29. Found: C, 34.72; H, 3.06; N, 10.15.

The purity of the used complexes is greater than 95% (>95%), as confirmed by elemental microanalysis and HPLC (high-performance liquid chromatography). The HPLC trace chromatograms and elemental microanalysis data are presented in the Supporting Information (Figures S21−S24).

Crystal Structure Determination. X-ray diffraction data for complex [Rh(bpma)Cl_3] (**Rh2**) were collected at room temperature using graphite-monochromated Mo Kα radiation (λ = 0.71073 Å) on

https://doi.org/10.1021/acs.jmedchem.4c01220
J. Med. Chem. 2024, 67, 13349−13362

an Oxford Diffraction Gemini S diffractometer. The CrysAlisPro and CrysAlis RED software packages were employed for data collection and data integration.[62] Final cell parameters were determined by a global refinement of 2215 reflections ($3.2° < q < 28.6°$). Space group determination was based on analysis of the Laue class and systematically absent reflections. Collected data for **Rh2** were corrected for absorption effects using the Multiscan method, applying an empirical absorption correction using spherical harmonics[63] as implemented in the SCALE3 ABSPACK[62] scaling algorithm.

Structure solution and refinement for **Rh2** were carried out with the programs SHELXT[64] and SHELXL-2018/3,[65] respectively. Molecular geometry calculations were performed by PLATON.[66] MERCURY[37] was employed for molecular graphics, and the OLEX2[67] software was used to prepare material for publication. Non-hydrogen atoms were refined freely with anisotropic displacement parameters. Hydrogen atoms attached to carbon atoms in phenyl rings and methylene groups were placed in geometrically idealized positions and refined as riding on their parent atoms, with C−H = 0.93 Å and $U_{iso}(H) = 1.2U_{eq}(C)$ and with C−H = 0.97 Å and $U_{iso}(H) = 1.5\ U_{eq}(C)$, respectively. Crystal data and experimental details of the structure determination are given in Tables S1 and S2.

Kinetic Studies. The kinetics of the coordinated chloride substitution were measured spectrophotometrically by following the change in absorbance at suitable wavelengths as a function of time. Working wavelengths were determined by recording the spectra of the reaction mixture from 220 to 450 nm. Kinetic measurements were performed under pseudo-first-order conditions. Reactions were initiated by mixing 0.50 mL of a nucleophile's complex solution with 2.50 mL of the thermally equilibrated complex solution in a UV−vis cuvette. Reactions were followed for at least 8 half-lives. The observed pseudo-first-order rate constants, k_{obsd}, represent an average value of three to four independent kinetic runs for each experimental condition. Values for constants and other thermodynamic parameters were determined by using Microsoft Excel 2010 and OriginPro 8.

Absorption Spectroscopic Studies. UV−vis spectrophotometric spectroscopy was used to determine the binding constant (K_b). The binding of complexes to DNA was performed at 37 °C. Phosphate buffer (0.01 M, pH = 7.4) was used for absorption measurements.

Ethidium bromide (EB) Displacement Studies. The fluorescence intensity was measured with the wavelength of excitation at 527 nm and the wavelength of emission at 612 nm. The width of the excitation and emission slits (10 nm) and scan rate were maintained constant throughout all experiments. The emission of the solution was recorded in the range of 550−750 nm. Interactions of the complex with DNA were studied in the presence of EB to determine whether the complex could replace EB from the DNA−EB complex. The DNA−EB complex was prepared by mixing 10 μM EB and 10 μM DNA (pH = 7.4). A series of solutions were prepared by mixing EB−DNA solutions with an increasing amount of complex. Possible effects of the complex binding to the DNA were studied by recording a change in the fluorescence emission spectrum after the addition of the complex solution.

Viscosity Measurements. DNA viscosity changes were assessed in the presence of rising concentrations of the investigated complexes, denoted as **Rh1−4**, both with and without selected ionic liquids (ILs) serving as cosolvents. Flow time was measured using a digital stopwatch three times for each sample to determine the average flow time. Data are presented as $(\eta/\eta^0)^{1/3}$ plotted against r, where η and η^0 represent the DNA viscosities observed in the presence of the complex and under buffer conditions, respectively. Viscosity quantifications were derived from the observed flow time of DNA-containing solutions (t) normalized against the flow time of buffer solely (t^0), expressed as $\eta = (t - t^0)/t^0$.

Lipophilicity Assay. The lipophilicity of **Rh1−4** complexes was determined utilizing the flask-shaking method.[68] The examined complexes were dissolved in dimethyl sulfoxide (DMSO) and subsequently introduced into the water/n-octanol system. Following this, the mixture underwent vortexing for a duration of 1 h at room temperature to facilitate partitioning. Subsequently, the solutions were left undisturbed for 24 h to enable phase separation. The concentrations of the complexes in both phases were determined by spectrophotometric analysis using previously established calibration curves. Logarithmic partition coefficients (log P) were computed employing the following formula:

$$\log P = \log(C^0/C^w)$$

where C^0 represents the concentration of the complex in n-octanol and C^w denotes the concentration in the aqueous phase.

Protein Binding Studies. The examination of interactions with human serum albumin (HSA) was conducted through the application of fluorescence spectroscopy. Spectra were recorded within the wavelength range 300−500 nm with the excitation wavelength set at 295 nm. The binding affinity of the investigated complex to the protein was discerned by monitoring alterations in the emission intensity of albumin (2 μM) subsequent to the incremental addition of the complex (0−10 μM). This method enabled the qualitative assessment of the binding effect with a particular focus on the diminishing emission intensity as a consequential outcome of the complex−protein interaction.

Molecular Docking Simulations. Molecular docking simulations have proven to be highly beneficial in predicting the atomic-level compatibility of small molecules and macromolecules. Scoring functions such as MolDock and Hbond, derived from Molegro Virtual Docker, can accurately measure the affinity between parent scaffolds and their integration complexes with target macromolecules. Moreover, the simulations' top-ranked poses provide valuable insights into the optimal positioning of the investigated complexes.

Structures of the investigated rhodium complexes were optimized and characterized as a local minimum (calculating vibration frequencies), using a B3LYP functional[69] in combination with the def2-SVP basis set[70,71] implemented in the GAUSSIAN suite program,[72] which was used just for optimizing the starting structures of the investigated rhodium complexes. These structures were docked into a rigid three-dimensional (3D) structural representation of canonical B-DNA (PDB ID: 1BNA), DNA with an intercalation gap (PDB ID: 1Z3F), HSA protein (PDB ID: 1AO6), tyrosyl-tRNA synthetase (PDB: 1JIJ), topoisomerase II DNA gyrase (PDB: 2XCT), and Bcl-2 protein (PDB ID: 2W3L). Structural coordinates of these macromolecules were obtained from the Protein Data Bank (PDB) (http://www.rcsb.org). If present, then all heteromolecules, ligands, and water molecules were removed. The docking was performed in a rigid structure of target macromolecules with flexible complex structures using Molegro Virtual Docker (MVD, version 2013.6.0.1).[73] Docking parameters were as follows: grid resolution of the binding side, 0.3 Å; maximum number of interactions, 1500; population size, 50; energy threshold, 100.00; and maximum number of steps, 300. A maximum population of 100 and a maximum number of interactions of 10 000 were used for each run. The search algorithm was MolDock SE, with the number of runs set to 100, and the number of generated poses at 10. The MVD-related scoring functions described the estimation of the investigated complexes' affinity to target macromolecules: MolDock, Docking, Rerank, and Hbond. Molegro scores were evaluated relatively (omitted from units, where the more negative values suggest greater binding prosperity of a complex to a macromolecule).[73] It is important to note that this approach of molecular docking simulation foremost presents the structural compatibility, emphasizing possible weak interactions, between selected macromolecules and investigated complexes and should be understood and discussed in that matter. It does not take into account the presence and therefore influence of the solvent and possible bond breaking and/or bond formatting which may occur during the experimental investigation of these interactions. Docked poses were visualized using the CHIMERA (http://www.cgl.ucsf.edu/chimera/) molecular graphics program.

In Vitro Cytotoxicity Study and Redox Status Modulation. This in vitro exploration focused on examining the cytotoxicity and principal redox status markers in human cervical cancer cells (HeLa) and normal lung-derived fibroblasts (MRC-5), which were sourced

https://doi.org/10.1021/acs.jmedchem.4c01220
J. Med. Chem. 2024, 67, 13349−13362

from the European Collection of Authenticated Cell Cultures. These cells were propagated in culture flasks, achieving approximately 80% confluence, under rigorous laboratory conditions compliant with Good Laboratory Practice (GLP) and a cell-centric approach to handling.

Cell viability was ascertained using the MTT assay, which relies on spectrophotometric measurement of the conversion of MTT to formazan, reflecting cellular metabolic activity. The cells, seeded in microplates, underwent a stabilization phase before treatment and were cultured in high-glucose DMEM with essential supplements. Viability percentages were calculated by comparing the absorbance of treated cells to that of the control group across a broad range of substance concentrations.

We quantified redox parameters, including superoxide anion radicals, nitrites, and glutathione (GSH), to evaluate the oxidative states induced by the substances. These parameters were determined spectrophotometrically at specific wavelengths for each compound with assays conducted at varying substance concentrations.

Statistical analyses were carried out with six replicates per dose, presenting the data as an average of two distinct experiments with the standard error. The relationship between variables was analyzed using the SPSS software, and the dose−response relationship was plotted to deduce the IC_{50} values, calculated via the CalcuSyn application. More details are available in our previously published studies.[23,35]

In Vitro Antimicrobial Assay. Test substances, microorganisms, and suspension preparation: the tested compounds were dissolved in DMSO and then diluted into a nutrient liquid medium to achieve a concentration of 10%. The antibiotics doxycycline (Galenika A.D., Belgrade) and fluconazole (Pfizer Inc., USA) were dissolved in Trypton Soy Broth (Torlak, Belgrade). The antimicrobial activity of four ligands and corresponding rhodium(III) complexes was tested for nine microorganisms including seven standard and clinical strains of pathogenic bacteria, one species of probiotic, and one clinical isolate yeast (Table S6). All clinical isolates were a generous gift from the Institute of Public Health, Kragujevac. The other microorganisms were provided from the collection held by the Microbiology Laboratory Faculty of Science, University of Kragujevac.

Bacterial and yeast suspensions were prepared by the direct colony method. The colonies were taken directly from the plate and were suspended in 5 mL of sterile 0.85% saline. The turbidity of the initial suspension was adjusted using a densitometer (DEN-1, BioSan, Latvia). When adjusted to the turbidity of a 0.5 McFarland standard, the bacteria suspension contained about 10^8 colony forming units (CFU)/mL and the suspension of yeast contained 10^6 CFU/mL. Ten-hold dilutions of the initial suspension were additionally prepared into sterile 0.85% saline.

Microdilution Method. Antimicrobial activity was tested by determining the minimum inhibitory concentration (MIC) and minimum microbicidal concentration (MMC) by using the microdilution plate method with resazurin.[74] The 96-well plates were prepared by dispensing 100 μL of Trypton Soy Broth into each well. A 100 μL portion from the stock solution of tested compound (concentration of 2000 μg/mL) was added into the first row of the plate. Then, 2-fold serial dilutions were performed by using a multichannel pipet. The obtained concentration range was from 1000 to 7.8 μg/mL. A 10 μL of diluted bacterial and yeast suspension was added to each well to give a final concentration of 5×10^5 CFU/mL for bacteria and 5×10^3 CFU/mL for yeast. Finally, 10 μL of resazurin solution was added to each well inoculated with bacteria and yeast. The inoculated plates were incubated at 37 °C for 24 h for bacteria and 28 °C for 48 h for the yeast. MIC was defined as the lowest concentration of the tested substance that prevented resazurin color change from blue to pink.

A solvent control test was performed to study the effect of 10% DMSO on the growth of microorganisms. It was observed that 10% DMSO did not inhibit the growth of the microorganisms. Doxycycline and fluconazole were used as positive control. Each test included a growth control and sterility control. All tests were performed in duplicate, and MICs were constant. The minimum bactericidal and fungicidal concentrations were determined by plating 10 μL of samples from wells, where no indicator color change was recorded, on nutrient agar medium. At the end of the incubation period, the lowest concentration with no growth (no colony) was defined as the minimum microbicidal concentration.

■ ASSOCIATED CONTENT

Supporting Information

The Supporting Information is available free of charge at https://pubs.acs.org/doi/10.1021/acs.jmedchem.4c01220.

Additional details of the experiments involving complexes **Rh1−4** including X-ray analyses; equations for kinetic studies and DNA binding studies using electronic absorption and fluorescence spectroscopic methods; docking studies and computational docking models of complexes **Rh1**, **Rh3**, and **Rh4** interacting with DNA and HSA; cytotoxicity and redox potential studies as well as assessments of ionic liquids and cotreatment effects; superoxide anion radical, nitrite, and glutathione production data; antimicrobial investigations of **Rh1−4** complexes; antimicrobial docking results with DNA Gyr and TyrRS enzymes; and HPLC chromatograms for **Rh1−4** complexes (PDF)

Complex's**Rh2** structure (CIF)

Molecular formula strings for **Rh1−4** and IL1−11 (CSV)

Rh1−1AO6(IIA) system (PDB)

Rh1−1AO6(IIIA) system (PDB)

Rh1−1BNA system (PDB)

Rh1−1JIJ system (PDB)

Rh1−1Z3F system (PDB)

Rh1−2XCT system (PDB)

Rh2−1AO6(IIA) system (PDB)

Rh2−1AO6(IIIA) system (PDB)

Rh2−1BNA system (PDB)

Rh2−1JIJ system (PDB)

Rh2−1Z3F system (PDB)

Rh2−2XCT system (PDB)

Rh3−1AO6(IIA) system (PDB)

Rh3−1AO6(IIIA) system (PDB)

Rh3−1BNA system (PDB)

Rh3−1JIJ system (PDB)

Rh3−1Z3F system (PDB)

Rh3−2XCT system (PDB)

Rh4−1AO6(IIA) system (PDB)

Rh4−1AO6(IIIA) system (PDB)

Rh4−1BNA system (PDB)

Rh4−1JIJ system (PDB)

Rh4−1Z3F system (PDB)

Rh4−2XCT system (PDB)

■ AUTHOR INFORMATION

Corresponding Author

Jovana Bogojeski − *University of Kragujevac, Faculty of Science, 34000 Kragujevac, Serbia;* orcid.org/0000-0002-3433-7774; Phone: +381 (0)34 336223; Email: jovana.bogojeski@pmf.kg.ac.rs; Fax: +381 (0)34 335040

Authors

Angelina Caković − *University of Kragujevac, Faculty of Science, 34000 Kragujevac, Serbia;* orcid.org/0000-0003-3909-4211

Dušan Ćoćić − *University of Kragujevac, Faculty of Science, 34000 Kragujevac, Serbia*
Marko Živanović − *University of Kragujevac, Institute for Information Technologies Kragujevac, Department of Science, 34000 Kragujevac, Serbia*
Nenad Janković − *University of Kragujevac, Institute for Information Technologies Kragujevac, Department of Science, 34000 Kragujevac, Serbia*
Nevena Milivojević − *University of Kragujevac, Institute for Information Technologies Kragujevac, Department of Science, 34000 Kragujevac, Serbia*
Marija Delibašić − *University of Belgrade, Faculty of Biology, Center for Forensic and Applied Molecular Genetics, 11000 Belgrade, Serbia;* orcid.org/0000-0002-4865-1334
Marina Kostić − *University of Kragujevac, Institute for Information Technologies Kragujevac, Department of Science, 34000 Kragujevac, Serbia*
Ivana Radojević − *University of Kragujevac, Faculty of Science, 34000 Kragujevac, Serbia*
Mirjana Grujović − *University of Kragujevac, Institute for Information Technologies Kragujevac, Department of Science, 34000 Kragujevac, Serbia*
Katarina G. Marković − *University of Kragujevac, Institute for Information Technologies Kragujevac, Department of Science, 34000 Kragujevac, Serbia*
Olivera R. Klisurić − *University of Novi Sad, Faculty of Sciences, Department of Physics, 21000 Novi Sad, Serbia*
Milan Vraneš − *University of Novi Sad, Faculty of Sciences, Department of Chemistry, Biochemistry and Environmental Protection, 21000 Novi Sad, Serbia;* orcid.org/0000-0001-8259-7549

Complete contact information is available at: https://pubs.acs.org/10.1021/acs.jmedchem.4c01220

Author Contributions

The manuscript was written through contributions of all authors.

Notes

The authors declare no competing financial interest.

■ ACKNOWLEDGMENTS

The authors gratefully acknowledge the financial support of the Ministry of Science, Technological Development and Innovation of the Republic of Serbia, Grants 451-03-66/2024-03/200122, 451-03-65/2024-03/200122, 451-03-47/2023-01/200378, 451-03-66/2024-03/200125, and 451-03-65/2024-03/200125.

■ ABBREVIATIONS USED

5′-GMP, guanosine-5′-monophosphate; CT-DNA, DNA from calf thymus; DMF, *N*,*N*-dimethylformamide; DNA, deoxyribonucleic acid; EB, ethidium bromide; ε_b, the extinction coefficient of a coordinated complex; ε_f, the extinction coefficient of an uncoordinated complex; GSH, glutathione; ^{1}H NMR, proton nuclear magnetic resonance spectroscopy; HCT-116, human colon cancer cell line; HSA, human serum albumin; IC_{50}, half-maximal inhibitory concentration; IL, ionic liquid; K_b, binding constant; K_{bin}, equilibrium binding constant; k_{obsd}, pseudo-first-order reaction rate constant; K_{sv}, Stern−Volmer constant; MRC-5, medical research council cell strain 5; PBS, phosphate buffered saline; ROS, reactive oxygen species; UV−vis, ultraviolet and visible spectrophotometry

■ REFERENCES

(1) Phillips, A. M. F.; Pombeiro, A. J. L. Tran-sition Metal-Based Prodrugs for Anti-cancer Drug Delivery. *Curr. Med. Chem.* **2020**, *26* (41), 7476−7519.
(2) Jia, P.; Ouyang, R.; Cao, P.; Tong, X.; Zhou, X.; Lei, T.; Zhao, Y.; Guo, N.; Chang, H.; Miao, Y.; Zhou, S. Review: Recent Advances and Future Development of Metal Complexes as Anticancer Agents. *J. Coord. Chem.* **2017**, *70* (13), 2175−2201.
(3) Nandanwar, S. K.; Kim, H. J. Anticancer and Antibacterial Activity of Transition Metal Complexes. *Chemistryselect* **2019**, *4* (5), 1706−1721.
(4) Hartmann, J. T.; Lipp, H. P. Toxicity of Platinum Compounds. *Expert Opin Pharmacother* **2003**, *4* (6), 889−901.
(5) Das, U.; Kar, B.; Pete, S.; Paira, P. Ru(Ii), Ir(III), Re(I) and Rh(III) Based Complexes as next Generation Anticancer Metallo-pharmaceuticals. *Dalton Trans* **2021**, *50*, 11259−11290.
(6) Da, W.; Jones, H. T.; Lin, J.-B.; Blight, B. A. Synthesis and Characterization of New Co(II), Rh(III), and Pt(II) Guanidine and Thiourea Complexes. *Can. J. Chem.* **2023**, *101* (03), 177−185.
(7) Štarha, P.; Trávníček, Z. Non-Platinum Complexes Containing Releasable Biologi-cally Active Ligands. *Coord. Chem. Rev.* **2019**, *395*, 130−145.
(8) Gupta, R. K.; Pandey, R.; Sharma, G.; Prasad, R.; Koch, B.; Srikrishna, S.; Li, P. Z.; Xu, Q.; Pandey, D. S. DNA Binding and Anti-Cancer Activity of Redox-Active Heteroleptic Piano-Stool Ru(II), Rh(III), and Ir(III) Complexes Containing 4-(2-Methoxypyridyl)-Phenyldipyrromethene. *Inorg. Chem.* **2013**, *52* (7), 3687−3698.
(9) Konkankit, C. C.; Marker, S. C.; Knopf, K. M.; Wilson, J. J. Anticancer Activity of Complexes of the Third Row Transition Metals, Rhenium, Osmium, and Iridium. *Dalton Trans* **2018**, *47* (30), 9934−9974.
(10) Hanif, M.; Babak, M. V.; Hartinger, C. G. Development of Anticancer Agents: Wizardry with Osmium. *Drug Discov Today* **2014**, *19* (10), 1640−1648.
(11) Máliková, K.; Masaryk, L.; Štarha, P. An-ticancer Half-Sandwich Rhodium(III) Complexes. *Inorganics* **2021**, *9* (4), 26.
(12) Geldmacher, Y.; Oleszak, M.; Sheldrick, W. S. Rhodium(III) and Iridium(III) Complexes as Anticancer Agents. *Inorg. Chim. Acta* **2012**, *393*, 84−102.
(13) Milutinović, M. M.; Bogojeski, J. V.; Klisurić, O.; Scheurer, A.; Elmroth, S. K. C.; Bugarčić, Ž. D. Synthesis and Structures of a Pincer-Type Rhodium(III) Complex: Reactivity toward Biomolecules. *Dalton Trans* **2016**, *45* (39), 15481−15491.
(14) Petrović, A.; Milutinović, M. M.; Petri, E. T.; Živanović, M.; Milivojević, N.; Puchta, R.; Scheurer, A.; Korzekwa, J.; Klisurić, O. R.; Bogojeski, J. Synthesis of Camphor-Derived Bis(Pyrazolylpyridine) Rhodium(III) Complexes: Structure-Reactivity Relationships and Biological Activity. *Inorg. Chem.* **2019**, *58* (1), 307−319.
(15) Esteghamat-Panah, R.; Hadadzadeh, H.; Farrokhpour, H.; Simpson, J.; Abdolma-leki, A.; Abyar, F. Synthesis, Structure, DNA/Protein Binding, and Cytotoxic Activity of a Rhodium(III) Complex with 2,6-Bis(2-Benzimidazolyl)Pyridine. *Eur. J. Med. Chem.* **2017**, *127*, 958−971.
(16) Liu, J. H.; Pan, F. H.; Wang, Z. F.; Wang, R.; Yang, L.; Qin, Q. P.; Tan, M. X. Synthesis, Crystal Structure and Biological Evaluation of Three New Rh(III) Complexes Incorporating Benzimidazole Derivatives. *Inorg. Chem. Commun.* **2020**, *118*, 108017.
(17) Mrkvicová, A.; Peterová, E.; Nemec, I.; Křikavová, R.; Muthná, D.; Havelek, R.; Kazimírová, P.; Řezáčová, M.; Štarha, P. Rh(III) and Ru(II) Complexes with Phosphanyl-Alkylamines: Inhibition of DNA Synthesis Induced by Anticancer Rh Complex. *Future Med. Chem.* **2023**, *15* (17), 1583−1602.
(18) Sohrabi, M.; Saeedi, M.; Larijani, B.; Mahdavi, M. Recent Advances in Biological Activities of Rhodium Complexes: Their Applications in Drug Discovery Research. *Eur. J. Med. Chem.* **2021**, *216*, 113308.
(19) Gu, Y.-Q.; Ma, M.-X.; Yang, Q.-Y.; Yang, K.; Li, H.-Q.; Hu, M.-Q.; Liang, H.; Chen, Z.-F. In Vitro and in Vivo Anticancer Activity of

Novel Rh(III) and Pd(II) Complexes with Pyrazolopyrimidine Derivatives. *Bioorg Chem.* **2023**, *141*, 106838.
(20) Pages, B. J.; Ang, D. L.; Wright, E. P.; Aldrich-Wright, J. R. Metal Complex In-teractions with DNA. *Dalton Trans* **2015**, *44* (8), 3505−3526.
(21) Boerner, L. J. K.; Zaleski, J. M. Metal Complex-DNA Interactions: From Transcription Inhibition to Photoactivated Cleavage. *Curr. Opin Chem. Biol.* **2005**, *9* (2), 135−144.
(22) Liu, H. K.; Sadler, P. J. Metal Complexes as DNA Intercalators. *Acc. Chem. Res.* **2011**, *44* (5), 349−359.
(23) Petrović, A.; Živanović, M.; Puchta, R.; Ćoćić, D.; Scheurer, A.; Milivojevic, N.; Bogojeski, J. Experimental and Quantum Chemical Study on the DNA/Protein Binding and the Biological Activity of a Rhodium(III) Complex with 1,2,4-Triazole as an Inert Ligand. *Dalton Trans* **2020**, *49* (26), 9070−9085.
(24) Reddy, B. S.; Sondhi, S. M.; Lown, J. W. Synthetic DNA Minor Groove-Binding Drugs. *Pharmacol Ther* **1999**, *84* (1), 1−111.
(25) Peng, B.; Gao, Z.; Li, X.; Li, T.; Chen, G.; Zhou, M.; Zhang, J. DNA Binding, DNA Cleavage and HSA Interaction of Several Metal Complexes Containing N-(2-Hydroxyethyl)-N′-Benzoylthiourea and 1,10-Phenanthroline Ligands. *J. Biol. Inorg. Chem.* **2016**, *21* (7), 903−916.
(26) Tzani, A.; Karadendrou, M. A.; Kalafateli, S.; Kakokefalou, V.; Detsi, A. Current Trends in Green Solvents: Biocompatible Ionic Liquids. *Crystals* **2022**, *12* (12), 1776.
(27) Jadhav, N. R.; Bhosale, S. P.; Bhosale, S. S.; Mali, S. D.; Toraskar, P. B.; Kadam, T. S. Ionic Liquids: Formulation Avenues, Drug Delivery and Therapeutic Updates. *J. Drug Deliv Sci. Technol.* **2021**, *65*, 102694.
(28) Gadilohar, B. L.; Shankarling, G. S. Cho-line Based Ionic Liquids and Their Applications in Organic Transformation. *J. Mol. Liq.* **2017**, *227*, 234−261.
(29) Pernak, J.; Syguda, A.; Mirska, I.; Pernak, A.; Nawrot, J.; Prádzyńska, A.; Griffin, S. T.; Rogers, R. D. Choline-Derivative-Based Ionic Liquids. *Chem. A Eur. J.* **2007**, *13* (24), 6817−6827.
(30) Pruchnik, F. P.; Jakimowicz, P.; Ciunik, Z.; Zakrzewska-Czerwińska, J.; Opolski, A.; Wietrzyk, J.; Wojdat, E. Rhodium(III) Complexes with Polypyridyls and Pyrazole and Their Antitumor Activity. *Inorg. Chim. Acta* **2002**, *334*, 59−66.
(31) Schmidtke, H.-H. Darstellung und Spektren einiger Rhodium-(III)-Komplexverbindungen. IV. Triacido-Triammin-Rhodium(III)-Verbindungen. *Z. Anorg. Allg. Chem.* **1965**, *339*, 103−112.
(32) Jaganyi, D.; Hofmann, A.; van Eldik, R. Controlling the Lability of Square-Planar Pt(II) Complexes through Electronic Communication between Pi-Acceptor Ligands. *Angew. Chem., Int. Ed. Engl.* **2001**, *40* (9), 1680−1683.
(33) Hofmann, A.; Jaganyi, D.; Munro, O. Q.; Liehr, G.; Van Eldik, R. Electronic Tuning of the Lability of Pt(II) Complexes through π-Acceptor Effects. Correlations between Thermodynamic, Kinetic, and Theoretical Parameters. *Inorg. Chem.* **2003**, *42* (5), 1688−1700.
(34) Vraneš, M.; Tot, A.; Papović, S.; Četo-jević-Simin, D.; Markov, S.; Velićanski, A.; Popsavin, M.; Gadžurić, S. Physico-chemical Features and Toxicity of Some Vitamin Based Ionic Liquids. *J. Mol. Liq.* **2017**, *247*, 411−424.
(35) Petrović, A. Z.; Ćoćić, D. C.; Bockfeld, D.; Živanović, M.; Milivojević, N.; Virijević, K.; Janković, N.; Scheurer, A.; Vraneš, M.; Bogojeski, J. V. Biological Activity of Bis(Pyrazolylpyridine) and Terpiridine Os(II) Complexes in the Presence of Biocompatible Ionic Liquids. *Inorg. Chem. Front* **2021**, *8* (11), 2749−2770.
(36) Vraneš, M. B.; Panić, J. J.; Tot, A. S.; Ostojić, S. M.; Četojević-Simin, D. D.; Janković, N.; Gadžurić, S. B. Synthesis and Thermophysical Characterization of New Biologically Friendly Agmatine-Based Ionic Liquids and Salts by Experimental and Computational Approach. *ACS Sustain Chem. Eng.* **2019**, *7* (12), 10773−10783.
(37) Bruno, I. J.; Cole, J. C.; Edgington, P. R.; Kessler, M.; Macrae, C. F.; McCabe, P.; Pearson, J.; Taylor, R. New Software for Searching the Cambridge Structural Data-base and Visualizing Crystal Structures. *Acta Crystallogr. B* **2002**, *58*, 389−397.
(38) Novakova, O.; Chen, H.; Vrana, O.; Rodger, A.; Sadler, P. J.; Brabec, V. DNA Interactions of Monofunctional Organometallic Osmium(II) Antitumor Complexes in Cell-Free Media. *Biochemistry* **2003**, *42*, 11544−11554.
(39) Long, E. C.; Barton, J. K. Demonstrating DNA Intercalation. *Acc. Chem. Res.* **1990**, *23* (9), 271−273.
(40) Pasternack, R. F.; Gibbs, E. J.; Villafranca, J. J. Interactions of Por-phyrins with Nucleic Acids. *Biochemistry* **1983**, *22* (23), 5409−5417.
(41) Koumousi, E. S.; Zampakou, M.; Rap-topoulou, C. P.; Psycharis, V.; Beavers, C. M.; Teat, S. J.; Psomas, G.; Stamatatos, T. C. First Palladium(II) and Platinum(II) Complexes from Employment of 2,6-Diacetylpyridine Dioxime: Synthesis, Structural and Spectroscopic Characterization, and Biological Evaluation. *Inorg. Chem.* **2012**, *51* (14), 7699−7710.
(42) Tarushi, A.; Polatoglou, E.; Kljun, J.; Turel, I.; Psomas, G.; Kessissoglou, D. P. Interaction of Zn(II) with Quinolone Drugs: Structure and Biological Evaluation. *Dalton Trans* **2011**, *40* (37), 9461−9473.
(43) Rizvi, M. A.; Zaki, M.; Afzal, M.; Mane, M.; Kumar, M.; Shah, B. A.; Srivastav, S.; Srikrishna, S.; Peerzada, G. M.; Tabassum, S. Nuclear Blebbing of Biologically Active Organoselenium Compound towards Hu-man Cervical Cancer Cell (HeLa): In Vitro DNA/HSA Binding, Cleavage and Cell Imaging Studies. *Eur. J. Med. Chem.* **2015**, *90* (2015), 876−888.
(44) Boger, D. L.; Fink, B. E.; Brunette, S. R.; Tse, W. C.; Hedrick, M. P. A Simple, High-Resolution Method for Establishing DNA Binding Affinity and Sequence Selectivity. *J. Am. Chem. Soc.* **2001**, *123* (25), 5878−5891.
(45) Dimiza, F.; Perdih, F.; Tangoulis, V.; Turel, I.; Kessissoglou, D. P.; Psomas, G. Interaction of Copper(II) with the Non-Steroidal Anti-Inflammatory Drugs Naproxen and Diclofenac: Synthesis, Structure, DNA- and Albumin-Binding. *J. Inorg. Biochem* **2011**, *105* (3), 476−489.
(46) Rippe, K. Analysis of Protein-DNA Binding at Equilibrium. *BIF futura* **1997**, *12*, 20−26.
(47) Jiang, M.; Li, Y. T.; Wu, Z. Y.; Liu, Z. Q.; Yan, C. W. Synthesis, Crystal Structure, Cytotoxic Activities and DNA-Binding Properties of New Binuclear Copper(II) Complexes Bridged by N,N′-Bis(N-Hydroxyethylaminoethyl)Oxamide. *J. Inorg. Biochem* **2009**, *103* (5), 833−844.
(48) Li, D. D.; Tian, J. L.; Gu, W.; Liu, X.; Yan, S. P. A Novel 1,2,4-Triazole-Based Copper(II) Complex: Synthesis, Characterization, Magnetic Property and Nuclease Activity. *J. Inorg. Biochem* **2010**, *104* (2), 171−179.
(49) He, X. M.; Carter, D. C. Atomic Structure and Chemistry of Human Serum Albumin. *Nature* **1992**, *358*, 209−2015.
(50) Steinhardt, J.; Krijn, J.; Leidy, J. G. Differences between Bovine and Human Serum Albumins: Binding Isotherms, Optical Rotatory Dispersion, Viscosity, Hydrogen Ion Titration, and Fluorescence Effects. *Biochemistry* **1971**, *10* (22), 4005−4015.
(51) Dömötör, O.; Enyedy, É. A. Binding Mechanisms of Half-Sandwich Rh(III) and Ru(II) Arene Complexes on Human Serum Albumin: A Comparative Study. *J. Biol. Inorg. Chem.* **2019**, *24* (5), 703−719.
(52) Espósito, B. P.; Najjar, R. Interactions of Antitumoral Platinum-Group Metallodrugs with Albumin. *Coord. Chem. Rev.* **2002**, *232*, 137−149.
(53) Al-Harthi, S.; Lachowicz, J. I.; Nowakowski, M. E.; Jaremko, M.; Jaremko, Ł. To-wards the Functional High-Resolution Co-ordination Chemistry of Blood Plasma Human Serum Albumin. *J. Inorg. Biochem* **2019**, *198*, 110716.
(54) Sathyadevi, P.; Krishnamoorthy, P.; Jayanthi, E.; Butorac, R. R.; Cowley, A. H.; Dharmaraj, N. Studies on the Effect of Metal Ions of Hydrazone Complexes on Interaction with Nucleic Acids, Bovine Serum Albumin and Antioxidant Properties. *Inorg. Chim. Acta* **2012**, *384*, 83−96.

https://doi.org/10.1021/acs.jmedchem.4c01220
J. Med. Chem. 2024, 67, 13349−13362

(55) Wang, F.; Huang, W.; Dai, Z. Spectroscopic Investigation of the Interaction between Riboflavin and Bovine Serum Albumin. *J. Mol. Struct.* **2008**, *875*, 509−514.
(56) Kasalović, M. P.; Petrović, A.; Živković, J. M.; Kuckling, L.; Jevtić, V. V.; Bogojeski, J.; Leka, Z. B.; Trifunović, S. R.; Pantelić, N. Evaluation of DNA/BSA Interactions and DFT Calculations of Gold(III), Zinc(II) and Palladium(II) Complexes with Triammonium N-Dithiocarboxyiminodiacetate. *J. Mol. Struct.* **2021**, *1229*, 129622.
(57) Paitandi, R. P.; Gupta, R. K.; Singh, R. S.; Sharma, G.; Koch, B.; Pandey, D. S. Interaction of Ferrocene Appended Ru(II), Rh(III) and Ir(III) Dipyrrinato Complexes with DNA/Protein, Molecular Docking and Antitumor Activity. *Eur. J. Med. Chem.* **2014**, *84*, 17−29.
(58) Song, Y.; Liu, Y.; Liu, W.; Villamena, F. A.; Zweier, J. L. Characterization of the Binding of the Finland Trityl Radical with Bovine Serum Albumin. *RSC Adv.* **2014**, *4* (88), 47649−47656.
(59) Esteghamat-Panah, R.; Hadadzadeh, H.; Farrokhpour, H.; Simpson, J.; Abdolma-leki, A.; Abyar, F. Synthesis, Structure, DNA/Protein Binding, and Cytotoxic Activity of a Rhodium(III) Complex with 2,6-Bis(2-Benzimidazolyl)Pyridine. *Eur. J. Med. Chem.* **2017**, *127*, 958−971.
(60) Senthil Raja, D.; Bhuvanesh, N. S. P.; Natarajan, K. Effect of N(4)-Phenyl Substitution in 2-Oxo-1,2-Dihydroquinoline-3- Carbaldehyde Semicarbazones on the Structure, DNA/Protein Interaction, and Antioxidative and Cytotoxic Activity of Cu(II) Complexes. *Inorg. Chem.* **2011**, *50* (24), 12852−12866.
(61) Andrejević, T. P.; Aleksic, I.; Počkaj, M.; Kljun, J.; Milivojevic, D.; Stevanović, N. L.; Nikodinovic-Runic, J.; Turel, I.; Djuran, M. I.; Glišić, B. Tailoring Copper(II) Complexes with Pyridine-4,5-Dicarboxylate Esters for Anti-: Candida Activity. *Dalton Trans* **2021**, *50* (7), 2627−2638.
(62) *CrysAlis PRO*; Rigaku Oxford Diffraction Ltd., Yarnton, Oxfordshire, England, 2015.
(63) Blessing, R. H. An Empirical Correction for Absorption Anisotropy. *Acta Cryst. A* **1995**, *51* (1), 33−38.
(64) Sheldrick, G. M. SHELXT - Integrated Space-Group and Crystal-Structure De-termination. *Acta Crystal A* **2015**, *71* (1), 3−8.
(65) Sheldrick, G. M. Crystal Structure Re-finement with SHELXL. *Acta Crystal C* **2015**, *71* (Md), 3−8.
(66) Spek, A. L. Structure Validation in Chem-ical Crystallography. *Acta Crystal D* **2009**, *65* (2), 148−155.
(67) Dolomanov, O. V.; Bourhis, L. J.; Gildea, R. J.; Howard, J. A. K.; Puschmann, H. OLEX2: A Complete Structure Solution, Refinement and Analysis Program. *J. Appl. Crystallogr.* **2009**, *42* (2), 339−341.
(68) Puckett, C. A.; Barton, J. K. Methods to Explore Cellular Uptake of Ruthenium Complexes. *J. Am. Chem. Soc.* **2007**, *129* (1), 46−47.
(69) Becke, A. D. Density-Functional Thermo-chemistry. III. The Role of Exact Exchange. *J. Chem. Phys.* **1993**, *98* (7), 5648−5652.
(70) Andrae, D.; Häußermann, U.; Dolg, M.; Stoll, H.; Preuß, H. Energy-Adjusted Ab Initio Pseudopotentials for the Second and Third Row Transition Elements. *Theor Chim Acta* **1990**, *77* (2), 123−141.
(71) Weigend, F.; Ahlrichs, R. Balanced Basis Sets of Split Valence, Triple Zeta Valence and Quadruple Zeta Valence Quality for H to Rn: Design and Assessment of Accuracy. *Phys. Chem. Chem. Phys.* **2005**, *7*, 3297−3305.
(72) Frisch, M. J.; Trucks, G. W.; Schlegel, H. B.; Scuseria, G. E.; Robb, M. A.; Cheeseman, J. R.; Scalmani, G.; Barone, V.; Mennucci, B.; Petersson, G. A.; Nakatsuji, H.; Caricato, M.; Li, X.; Hratchian, H. P.; Izmaylov, A. F.; Bloino, J.; Zheng, G.; Sonnenberg, J. L.; et al. *Gaussian 09 Revision C.01*; Gaussian, Inc., Wallingford CT, 2010.
(73) Khan, T.; Sankhe, K.; Suvarna, V.; Sherje, A.; Patel, K.; Dravyakar, B. DNA Gyrase Inhibitors: Progress and Synthesis of Potent Compounds as Antibacterial Agents. *Biomedicine and Pharmacotherapy* **2018**, *103*, 923−938.
(74) Sarker, S. D.; Nahar, L.; Kumarasamy, Y. Microtitre Plate-Based Antibacterial Assay Incorporating Resazurin as an Indicator of Cell Growth, and Its Application in the in Vitro Antibacterial Screening of Phytochemicals. *Methods* **2007**, *42* (4), 321−324.

https://doi.org/10.1021/acs.jmedchem.4c01220
J. Med. Chem. 2024, 67, 13349−13362